Compositional heterogeneity of insoluble organic matter extracted from asteroid Ryugu samples

Eric Quirico, Lydie Bonal, Yoko Kebukawa, Kana Amano, Hikaru Yabuta, Van Phan, Pierre Beck, Laurent Rémusat, Emmanuel Dartois, Cecile Engrand, et al.

The Meteoritical Society

Meteoritics & Planetary Science 59, Nr 8, 1907–1924 (2024)
doi: 10.1111/maps.14097

Compositional heterogeneity of insoluble organic matter extracted from asteroid Ryugu samples

Eric QUIRICO[1]*, Lydie BONAL[1], Yoko KEBUKAWA[2], Kana AMANO[3], Hikaru YABUTA[4], Van T. H. PHAN[1], Pierre BECK[1], Laurent RÉMUSAT[5], Emmanuel DARTOIS[6], Cecile ENGRAND[7], Zita MARTINS[8], Laure BEJACH[7], Alexandre DAZZI[9], Ariane DENISET-BESSEAU[9], Jean DUPRAT[5], Jérémie MATHURIN[9], Gilles MONTAGNAC[10], Jens BAROSCH[11], George D. CODY[11], Bradley DE GREGORIO[12], Yuma ENOKIDO[3], Minako HASHIGUCHI[13], Kanami KAMIDE[4], David KILCOYNE[14], Mutsumi KOMATSU[15,16], Megumi MATSUMOTO[3], Smail MOSTEFAOUI[5], Larry NITTLER[11], Takuji OHIGASHI[17], Taiga OKUMURA[18], Scott SANDFORD[19], Miho SHIGENAKA[4], Rhonda STROUD[12], Hiroki SUGA[20], Yoshio TAKAHASHI[18], Yasuo TAKEICHI[21], Yusuke TAMENORI[20], Maximilien VERDIER-PAOLETTI[5], Daisuke WAKABAYASHI[21], Shohei YAMASHITA[21], Tomoki NAKAMURA[3], Hiroshi NARAOKA[22], Takaaki NOGUCHI[22], Ryuji OKAZAKI[22], Hisayoshi YURIMOTO[23], Kanako SAKAMOTO[24], Shogo TACHIBANA[18,23], Sei-Ichiro WATANABE[13], Yuichi TSUDA[23], Toru YADA[24], Masahiro NISHIMURA[24], Aiko NAKATO[24], Akiko MIYAZAKI[24], Kasumi YOGATA[24], Masanao ABE[24], Tatsuaki OKADA[24], Tomohitro USUI[24], Makoto YOSHIKAWA[24], Takanao SAIKI[24], Satoshi TANAKA[24], Fuyuto TERUI[25], and Satoru NAKAZAWA[24]

[1]Institut de Planétologie et d'Astrophysique (IPAG), UMR 5274, CNRS, Université Grenoble Alpes, Grenoble, France
[2]Department of Chemistry and Life Science, Yokohama National University, Yokohama, Japan
[3]Department of Earth Science, Tohoku University, Sendai, Japan
[4]Department of Earth and Planetary Systems Science, Hiroshima University, Hiroshima, Japan
[5]Institut de Minéralogie, Physique des Matériaux et Cosmochimie, Museum National d'Histoire Naturelle, Centre National de la Recherche Sientifique, Sorbonne Université, Paris, France
[6]Institut des Sciences Moléculaires d'Orsay, Centre National de la Recherche Scientifique, Université Paris-Saclay, Orsay, France
[7]Laboratoire de Physique des 2 Infinis Irène Joliot-Curie, Université Paris-Saclay, Centre National de la Recherche Scientifique, Orsay, France
[8]Centro de Química Estrutural, Institute of Molecular Sciences and Department of Chemical Engineering, Instituto Superior Técnico, Universidade de Lisboa, Lisbon, Portugal
[9]Institut Chimie Physique, Centre National de la Recherche Scientifique, Université Paris-Saclay, Orsay, France
[10]ENS de Lyon, Univ Lyon 1, CNRS, LGL-TPE, Université de Lyon, Lyon, France
[11]Earth and Planets Laboratory, Carnegie Institution for Science, Washington, DC, USA
[12]Materials Science and Technology Division, US Naval Research Laboratory, Washington, DC, USA
[13]Graduate School of Environmental Studies, Nagoya University, Nagoya, Japan
[14]Advanced Light Source, Lawrence Berkeley National Laboratory, Berkeley, California, USA
[15]Center for University-Wide Education, Saitama Prefectural University, Saitama, Japan
[16]Department of Earth Sciences, Waseda University, Tokyo, Japan
[17]Institute for Molecular Science, UVSOR Synchrotron Facility, Okazaki, Japan
[18]Department of Earth and Planetary Science, The University of Tokyo, Tokyo, Japan
[19]NASA Ames Research Center, Moffett Field, California, USA
[20]Japan Synchrotron Radiation Research Institute, Hyogo, Japan
[21]Institute of Materials Structure Science, High Energy Accelerator Research Organization, Tsukuba, Japan
[22]Department of Earth and Planetary Sciences, Kyushu University, Fukuoka, Japan
[23]Department of Earth and Planetary Sciences, Hokkaido University, Sapporo, Japan
[24]Institute of Space and Astronautical Science, Japan Aerospace Exploration Agency (JAXA), Sagamihara, Japan
[25]Kanagawa Institute of Technology, Atsugi, Japan

*Correspondence
Eric Quirico, Institut de Planétologie et d'Astrophysique (IPAG), UMR 5274, CNRS, Université Grenoble Alpes, Grenoble F-38041, France.
Email: eric.quirico@univ-grenoble-alpes.fr

(Received 10 April 2023; revision accepted 13 September 2023)

Abstract–We report a Fourier transform infrared analysis of functional groups in insoluble organic matter (IOM) extracted from a series of 100–500 μm Ryugu grains collected during the two touchdowns of February 22 and July 11, 2019. IOM extracted from most of the samples is very similar to IOM in primitive CI, CM, and CR chondrites, and shows that the extent of thermal metamorphism in Ryugu regolith was, at best, very limited. One sample displays chemical signatures consistent with a very mild heating, likely due to asteroidal collision impacts. We also report a lower carbonyl abundance in Ryugu IOM samples compared to primitive chondrites, which could reflect the accretion of a less oxygenated precursor by Ryugu. The possible effects of hydrothermal alteration and terrestrial weathering are also discussed. Last, no firm conclusions could be drawn on the origin of the soluble outlier phases, observed along with IOM in this study and in the preliminary analysis of Ryugu samples. However, it is clear that the HF/HCl residues presented in this publication are a mix between IOM and the nitrogen-rich outlier phase.

INTRODUCTION

Between June 2018 and November 2019, the C-type asteroid Ryugu has been surveyed by the Hayabusa 2 spacecraft, operated by the Japan Aerospace Exploration Agency (JAXA). Extensive remote sensing characterizations have been achieved, both from the spacecraft and the Mobile Asteroid Surface Scout (MASCOT) lander, providing a plethora of unprecedented information about surface and subsurface morphology and composition (Kitazato et al., 2019; Sugita et al., 2019; Watanabe et al., 2019). Touchdowns at two different sites were achieved on February 22 and July 11, 2019, leading to the collection of 5.42 g of highly valuable surface material (Yada et al., 2022). These samples were brought back to Earth on December 2020 and were analyzed during 1 year by the Hayabusa2 initial analysis team (IAT), consisting of six specialized subteams.

Ryugu samples are a unique opportunity for enlightening on the link between meteorites and asteroids, as their parent body is clearly identified and they have escaped contamination and oxidation from the terrestrial environment, at odds with most of chondrites collected on Earth. Note that Okazaki et al. (2022) reported the presence of 70 Pa of air in the sample container, meaning that the samples were exposed to ~35 Pa of air during ~30 h. This corresponds to an O_2 partial pressure of 7×10^{-4} bar, which is not enough to oxidize insoluble organic matter (IOM; ~months are required to oxidize IOM under air in the laboratory) and to oxidize minerals, for example, very reactive sulfides (see Nakamura et al., 2022 for a thorough discussion).

Analyses published so far have revealed a material sharing strong similarities with CI chondrites (Nakamura et al., 2022; Yokoyama et al., 2023), with limited extents of hydrothermal alteration and space weathering (Noguchi et al., 2023; Yokoyama et al., 2023). The bulk carbon abundance in the samples lies between 3 and 6.8 wt% (Ito et al., 2022; Naraoka et al., 2023; Okazaki et al., 2022; Yokoyama et al., 2023), about one-third of which is detected in the form of both IOM and soluble organic matter (SOM; Yokoyama et al., 2023). Yabuta et al. (2023) presented extensive analyses of organics in bulk grains and two IOM samples, extracted from materials collected during the two touchdowns. They show that Ryugu samples share similarities with primitive carbonaceous chondrites, in terms of organic composition and morphology, but also differences that are not yet fully understood. In particular, HF/HCl acid extractions led to residues different from IOM extracted from primitive chondrites, especially a higher CH_2/CH_3 ratio. Kebukawa et al. (2023) have further discussed the interpretation of infrared spectra of IOM and reported the spectra of a yellowish translucent phase that was collected along with IOM after extraction. This phase, named *outlier carbonaceous phases*, is nitrogen-rich and very different from polyaromatic IOM usually extracted from chondrites. Infrared organic features have also been reported by Dartois et al. (2023) in intact Ryugu particles, as carbonyl, aromatic C=C, and aliphatic

groups with a higher CH_2/CH_3 than generally measured in IOM from C1 chondrites.

In this study, we report an infrared analysis of functional groups of IOM samples extracted from a series of submillimeter grains from A and C collectors, corresponding to the two touchdowns of February 22 and July 11, 2019, respectively. We question the chemical composition variations across and within the samples, the link toward CI chondrites, and the implications about the past presence of thermal processes in Ryugu regolith. Such thermal events have been evidenced with a significant prevalence in C1 an C2 chondrites and may have been triggered by impacts (e.g., Nakamura, 2005; Quirico et al., 2018; Tonui et al., 2014). We also discuss the possible effects of oxidation triggered by hydrothermal alteration and terrestrial weathering. Last, we compare our data and results with those reported in Yabuta et al. (2023) and Kebukawa et al. (2023), and focus on the composition of *outlier carbonaceous phases* that were also recovered in some of our own extractions.

SAMPLES AND EXPERIMENTAL PROCEDURES

Samples are submillimeter grains separated from the individual grain C0057-6 (0.9 mg) and particles from the three aggregates A0106 (38.4 mg), A0108 (3.5 mg), and C0109 (3.7 mg; Table 1). Here, *individual grain* refers to an intact Ryugu particle, and *aggregate* refers to a collection of small millimeter-sized grains that were gathered after being picked up in the curation center at JAXA. Aggregates are then made of intact grains which were not spatially associated in the regolith.

Eleven IOM samples were extracted by acid etching following the protocol of Durand and Nicaise (1980), adapted to submillimeter samples (Orthous-Daunay et al., 2010; Quirico et al., 2018; Table 1). The experimental setup includes a PTFE HPLC filter holder with a PTFE filter (pore size 0.2 μm; Figure 1). In order to prevent any leaking of reagents, the sample holder was tightly maintained between two metallic parts with six screws. Fluids were circulated through Viton and PTFE wires with a peristaltic pump (Ismatec®; flow rate of 94 μL min^{-1}). All operations were run under an inert atmosphere (argon). The grains were transferred onto a PTFE filter, beforehand wet with ethanol to prevent grain loss due to static electricity. Microhandling was operated with a tungsten needle under a binocular microscope, in an ISO2 clean room equipped with an ISO4 laminar hood.

The chemical protocol comprised the following stages (Figure 2). (1) Ultrapure water (Milli-Q water, 18.2 MΩ) and CH_3OH:CH_3Cl (2/1 v/v) leaching sequences were applied to extract soluble organic molecules (hereafter SOM). (2) HCl 6N was used to remove carbonates, sulfides (pyrrhotite and pentlandite), and other minerals, as one step of 2 h, followed by ultrapure water rinsing and a second step overnight. (3) A similar sequence with HF (48%):HCl (37%) (2/1 v/v) was run, followed by a short HCl 6N sequence (2 h), to remove any cations that might subsequently react with F^- to form insoluble fluorides. (4) The sample was rinsed again with ultrapure water and CH_3OH:CH_3Cl (2/1 v/v), for removing encaged free molecules. (5) After having purged the remaining reagents, the sample holder was dismounted and the filter was dried. We observed that individual grains deposited on the filter were not fragmented and looked like platelets. This resulted from the subtraction of mineral from the initial grains and the collapse of insoluble organic material.

TABLE 1. Samples investigated.

Sample	Grain size (μm)	FT-IR-residue	FT-IR-bulk	I_{CH_2}/I_{CH_3}
A0108-6,10	~100	y	y	
A0108-18	—	n	y	
A0106-4	~500	y		x
A0106-6	~500	y		x
A0106-23,24,25	~500	y		
A0108-61	~500	y		
A0108-60	~500	y		x
C0057-6	~500	y		x
C0109-5	~500	Opaque		
C0109-9	~500	y		x
C0109-12	~500	Scattering	y	
Orgueil	100–1000	y		x

Note: A0106-23,24,25 was a set of three particles on the same glass slide, which were mixed during transportation and could not distinguished. A0108-6,10 consists of two particles that could not be distinguished after manipulation. Scattering: IR light scattering prevents from collecting spectra of good quality. Opaque: the IR beam did not pass through the sample.

A0108-6 and A0108-10 were extracted from bulk grains of ~100 μm across, leading to very tiny IOM grains. After crushing IOM samples between two diamond windows, these windows were separated and analyzed separately. We observed dark and red-brown translucent regions. Infrared spectra could be collected from the later, while the dark region was fully opaque to infrared radiations. Other IOM samples were obtained from larger grains (~500 μm across) and thicker samples were obtained after crushing them between diamond windows. C0109-5 was found totally opaque to infrared radiations and was characterized by scanning electron microscopy (FEG-SEM Carl ZEISS NVISION 40, CEA/CMTC Université Grenoble Alpes; Figure 3). Images reveal a high abundance of Fe-Ni sulfides over a range of scale from several tens of nm to several micrometers (including subhedral crystals).

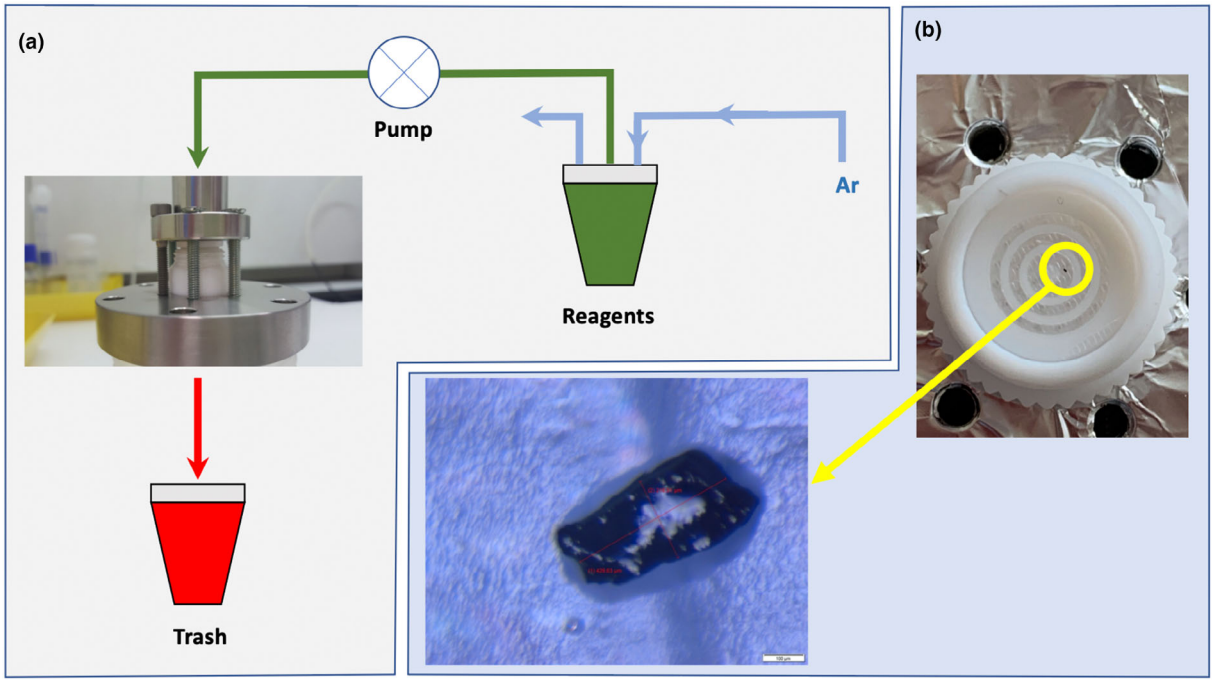

FIGURE 1. Schematic of the experimental setup used to extract IOM residues from submillimeter grains. (a) A PTFE filter holder was maintained between two stainless steel parts tightly pressed with six screws. Reagents were circulated with a peristaltic pump under an inert atmosphere (Argon). (b) The PTFE filter loaded with an ~500 μm sample before extraction. (Color figure can be viewed at wileyonlinelibrary.com)

Infrared spectra were collected with a Bruker Hyperion 3000 infrared microscope equipped with a MCT detector cooled with liquid nitrogen. The infrared beam was focused with a 15× objective, and the typical size of the spot onto the sample was between 50 × 50 and 100 × 100 μm^2. The spectral resolution was 4 cm^{-1} and the spectral range was 4000–650 cm^{-1}. IOM samples were picked off and transferred on a 3 × 0.5 mm synthetic type IIa diamond window, and then crushed using another window in a homemade press (Battandier et al., 2018). Both windows were then transferred into an environmental cell maintained under secondary vacuum (~10^{-6} mbar) and gentle heating (~80°C) to remove adsorbed atmospheric molecular water. The spectra were processed with the Igor Pro 8.04 software (Wavemetrics Inc.). Baseline corrections were processed with spline functions. All spectra were normalized by setting the absorbance of the peak of the 1600 cm^{-1} band to 1.

We also collected measurements on the two IOM samples obtained from A0106 and C0107 aggregates by Yabuta et al. (2023) (hereafter, Y23-A0106-IOM and Y23-C0107-IOM). They were extracted following the HF/HCl protocol with a device optimized to samples of 1–10 mg. The main differences with the protocol of our study are a longer time of the samples in the acid solutions, and the need of different steps of centrifugation and supernatant removal. Finally, spectra were also collected on intact particles (particles A0108-6, -10, and -18).

AFM-IR measurements were collected using a nanoIR3s™ (Bruker) at IPAG (Grenoble, France). An atomic force microscope (AFM) tip is used to scan the sample and to generate topographic images, as well as measuring IR absorption by detecting the photothermal expansion triggered by a tunable laser. Detailed descriptions of the NanoIR3s™ (Bruker) have been provided in previous publications (e.g., Phan et al., 2022, 2023). Basically, the nanoIR3s™ is equipped with two tunable pulsed lasers providing infrared light in the 700–2000 cm^{-1} region, supplied by an OPO/DFG (optical parametric oscillator and a difference frequency generation) architecture (APE, GmbH, Germany). The tapping (TM) and contact mode (CM) were used for punctual and imaging spectroscopy, respectively. The laser background was collected prior to collecting images and/or spectra and the laser alignment optimization was performed prior to signal acquisition at different frequencies within the scanned frequency range.

AFM-IR images were recorded using the tapping IR mode with a laser power of 8.81%–40%, and a pulse rate of at 340–370 kHz to avoid physical damage of the probe on the sample surface (Phan et al., 2022, 2023). AFM-IR images through the region of interest (ROI) were collected from each section at infrared wave number of

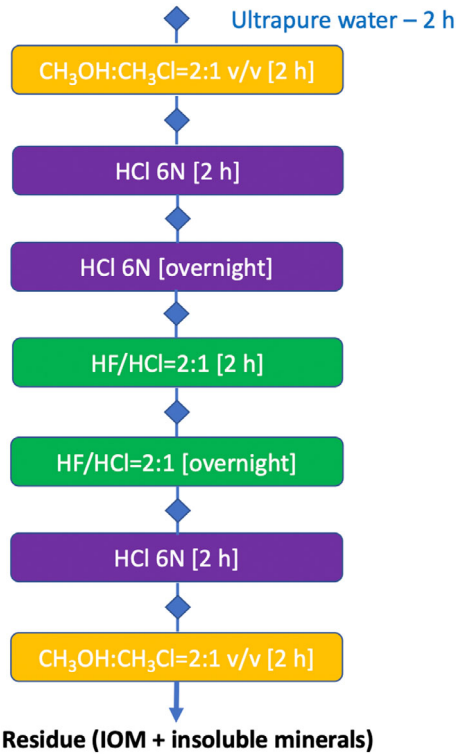

FIGURE 2. The different steps of the HF/HCl digestion protocol. The full sequence lasts ~4 days. (Color figure can be viewed at wileyonlinelibrary.com)

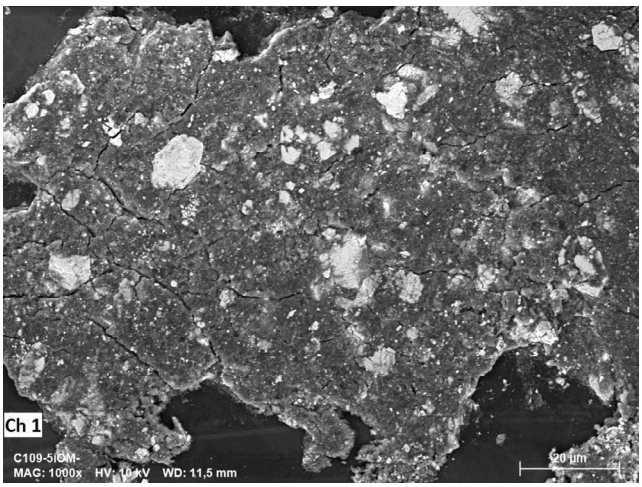

FIGURE 3. Backscattered electrons image of the acid residue extracted from C0109-5. Bright inclusions are Ni-rich Fe-sulfides that cover a range of size from tens of nanometer to several micrometers. This residue was fully opaque to visible and infrared radiations.

1720, 1600, 1450, 1150, and 1050–1000 cm^{-1} corresponding to carbonyl (C = O) stretching, sp^2 aromatic (C = C), carbonate (CO_3) and (CH_2) bending mode, sulfate and silicate (Si-O) stretching mode, respectively. The composite RGB color images were generated through combining three different absorption images using the Anasys software to emphasize the spatial distribution of different chemical groups or minerals. Before overlying them, realignment was done to compensate for any small drifts between each AFM-IR image recording. The scan speed of all maps was 0.1 Hz and the scan sizes ranged 300 × 300 to 500 × 500 points, depending on the size of the ROI.

Local AFM-IR spectra were collected in contact mode after collection of AFM-IR image in tapping mode. In fact, local spectra were also performed in tapping mode but the signal to noise ratio was not of the same quality as in contact mode. Therefore, we only describe below contact AFM-IR spectra. The incident laser powers were set to 1.22%–5.03%, with a pulse rate of 240–300 kHz to avoid damaging samples, while obtaining good quality spectra. The IR spectra were optimized at a constant laser power level for each wave number, with the laser power detected by an IR sensitive photodetector. Each AFM-IR spectrum was obtained at selected points with a wave number spacing of 4 cm^{-1} and we have used co-averages of three spectra. The AFM probe is the gold-coated semi-tap probe (PR-EX-TnIR-A-10, 75 ± 15 kHz, 1–7 N m^{-1}), which can avoid artifact effects due to the silicon IR absorption and allow to work both in contact and tapping AFM-IR modes.

RESULTS

Residues Resembling Chondritic IOM

Infrared spectra of IOM samples are displayed in Figures 4 and 5. The IOM samples extracted from 500 µm Ryugu grains look similar to those from type 1 and 2 chondrites, and in particular Orgueil, Ivuna, and Alais (Kebukawa et al., 2011; Orthous-Daunay et al., 2013; Quirico et al., 2018). A broadband with peaks at 2856, 2873, 2923, 2950 cm^{-1} is observed in the range 2800–3000 cm^{-1}. It is controlled by the symmetric and antisymmetric stretching modes of the CH, CH_2, and CH_3 groups, with complex interactions with overtones from fundamental vibrations. Theoretical studies and low-temperature measurements reveal up to eight different vibration modes (MacPhail et al., 1984). Usually, in practice, the above-mentioned peaks are assigned to symmetric and antisymmetric stretching modes of CH_2 and CH_3, and a component at ~2900 cm^{-1} due to the contribution of a Fermi resonance and/or of C-H groups is usually introduced in the fit models (Dartois et al., 2005; Orthous-Daunay et al., 2013). The broadband at 3660 cm^{-1} can be assigned either to residual atmospheric moisture trapped in closed porosity, or to hydroxyl groups as alcohol or carboxylic groups in the macromolecular structure. This

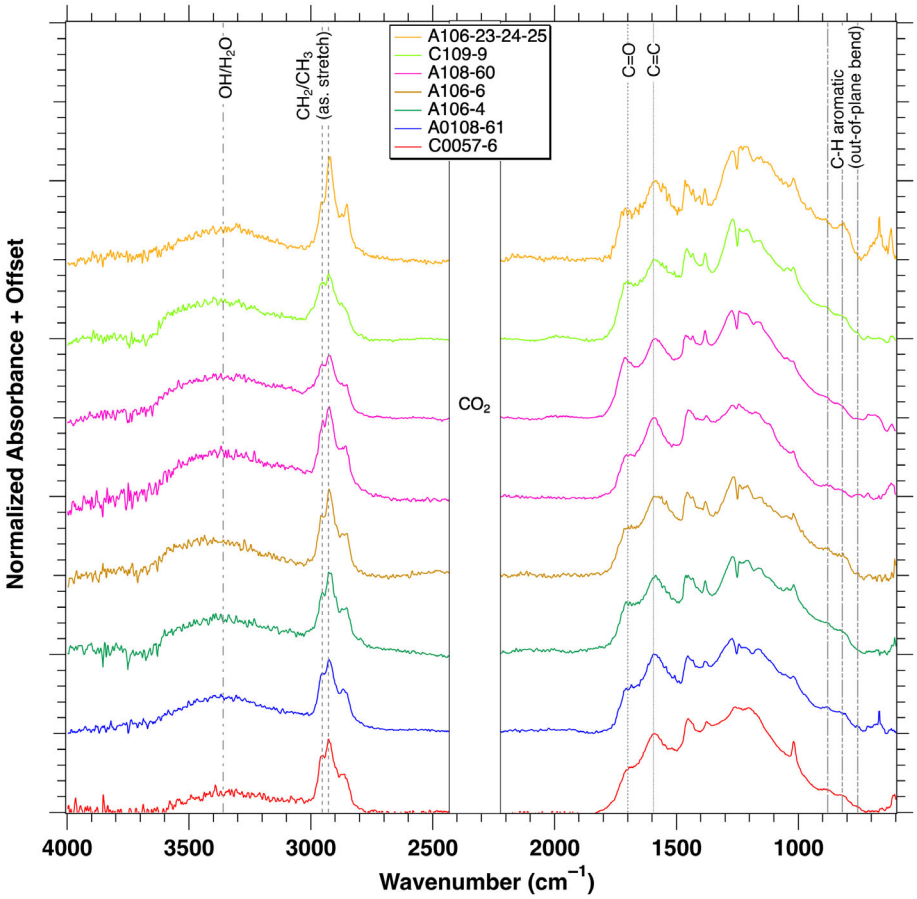

FIGURE 4. IOM baseline-corrected spectra of various aggregates and intact grains. (Color figure can be viewed at wileyonlinelibrary.com)

band may be difficult to observe if interference fringes modulate the baseline of the spectra. Note that the weak intensity of this feature supports the low abundance of these groups. The bands at ~1590 and ~1700 cm^{-1} are assigned to the C = C stretching mode of polyaromatic units and to the stretching vibration mode of the carbonyl C = O group (Table 2; Chen et al., 2012; Painter et al., 1981; Petersen et al., 2008). The bands at ~1450, 1430, and 1380 cm^{-1} are assigned to CH_2 and CH_3 deformation modes, as scissoring for CH_2, and symmetric and antisymmetric bending modes for CH_3 (Lin-Vien et al., 1991). The broad feature extending from 1500 to 800 cm^{-1} is highly congested, and no functional group can be unambiguously identified (Painter et al., 1981). Several weak bands at 1020 cm^{-1} and below are not clearly identified, and could be due to out of plane C-H bending in aromatics, wagging, twisting, and rocking modes in methyl and methylene groups.

Three spectral parameters were calculated for each spectrum:

1. I_{as-CH_2}/I_{as-CH_3}, as the ratio of the peak intensity of the 2950 and 2923 cm^{-1} components of the aliphatic band, corresponding to the antisymmetric stretching modes of the CH_2 and CH_3 groups. A linear local baseline was applied in the range 2700–3050 cm^{-1}.
2. $I_{C=O}/I_{C=C}$ as the peak intensity of the carbonyl band at 1700 cm^{-1} as the intensity of the C=C band is normalized to 1 in all spectra.
3. The integrated absorbance of the aliphatic band, as:

$$A_{ali} = \int_{2700}^{3040} \mathrm{abs}(\nu)\mathrm{d}\tilde{\nu}$$

where $\tilde{\nu}$ is the wave number, and abs the absorbance.

The spectra collected from Ryugu particles can then be semiquantitatively compared to the spectra of the three CI historical chondrites Alais, Ivuna, and Orgueil, and to IOM from other primitive chondrites that were analyzed in previous publications (Orthous-Daunay et al., 2013; Quirico et al., 2018; Figure 6).

We also attempted the full quantification of IOM spectra through spectral decomposition, using published band strengths (Dartois et al., 2004, 2013; Orthous-Daunay et al., 2013; Phan et al., 2021). It turned out that the spectral decomposition in the range 2000–950 cm^{-1}

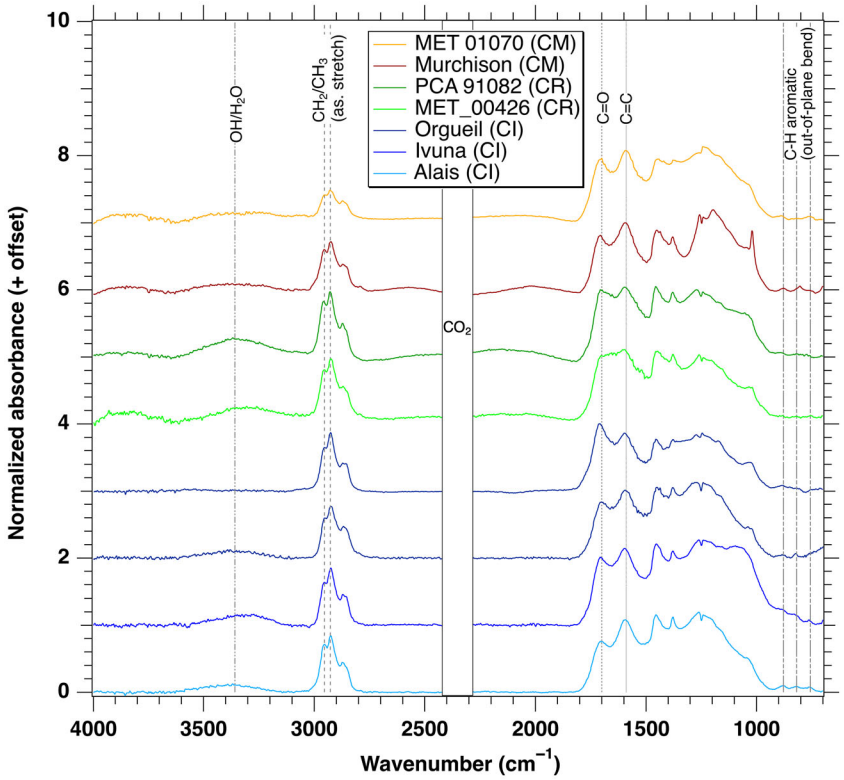

FIGURE 5. IOM baseline-corrected spectra of CI, CM, and CR chondrites. Spectra from Orthous-Daunay et al. (2013) and Quirico et al. (2018), except for Orgueil (this study). (Color figure can be viewed at wileyonlinelibrary.com)

TABLE 2. Band positions and assignment in the spectra of IOM samples.

Samples	OH/H_2O (cm^{-1})	CH_3-as (cm^{-1})	CH_2-as (cm^{-1})	CH_3-s (cm^{-1})	CH_2-s (cm^{-1})	C = O (cm^{-1})	C = C (cm^{-1})	CH_3 and CH_2-d (cm^{-1})		
A0106-23-24-25	3360 ± 20	2950 ± 4	2921 ± 4	2867 ± 1	2852 ± 2	1714 ± 8	1589 ± 2	1458 ± 3	1431 ± 3	1383 ± 2
C0109-9	3360 ± 20	2952 ± 2	2927 ± 1	—	—	1704 ± 4	1593 ± 2	1456 ± 3	1433 ± 3	1383 ± 2
A0108-60 (1)	3360 ± 20	2952 ± 2	2923 ± 2	—	—	1710 ± 2	1587 ± 2	1462 ± 3	1433 ± 3	1383 ± 2
A0108-60 (2)	3360 ± 20	2953 ± 1	2927 ± 2	—		1707 ± 3	1595 ± 2	1452 ± 3	—	1377 ± 2
A0106-6	3360 ± 20	2958 ± 2	2925 ± 2	2871 ± 2	2852 ± 2	1700 ± 8	1581 ± 4	1456	1433	1381
A0106-4	3360 ± 20	2952 ± 4	2923 ± 4	2871 ± 4	2854 ± 4	1701 ± 6	1585 ± 3	1460	1433	1383
A0108-61	3360 ± 20	2953 ± 1	2927 ± 1	2867 ± 1	2853 ± 1	1701 ± 8	1589 ± 2	1454	1433	1383
C0057-6	3360 ± 20	2952 ± 2	2925 ± 2	2867 ± 2	2852 ± 2	1701 ± 8	1595 ± 2	1452	1433	1377
Outlier IOM	3248 ± 5	2957 ± 1	2922 ± 2	—	2850 ± 2	1703 ± 6	—	—	—	—
A0108-6,10	3360 ± 20	—	2921 ± 2	—	2850 ± 2	1707 ± 6	1608 ± 5	—	—	—

Abbreviations: as, asymmetric stretching; d, deformation modes, that is, scissoring for CH_2, symmetric and asymmetric bending for CH_3; s, symmetric stretching; —, lacking or position determination impossible.

has no unique solution. Different fit models lead to a good fit (in terms of X^2 minimization). Due to the spectral congestion, the exact number of spectral components cannot be determined accurately. For instance, for the same spectrum of Orgueil IOM, a very good fit led to integrated absorbances of the C = C and C = O band of 131 and 57 cm^{-2}, respectively, against 106 and 86 cm^{-2} obtained by fitting with different initial parameters. These differences of ~30% for each band result in a factor of 2 when calculating the $N_{C=O}/N_{C=C}$. This uncertainty is very high, and we did not pursue this quantification. As mentioned before, no spectra could be collected from the IOM of particle C0109-5. The spectra of C0109-12 looked significantly disturbed by scattering, and we preferred to put aside these data.

The values of semiquantitative parameters I_{as-CH_2}/I_{as-CH_3}, $I_{C=O}/I_{C=C}$, and A_{ali} are displayed in Figure 6. A0106-4, A0106-6, A0108-60, A0108-61, C0057-6,

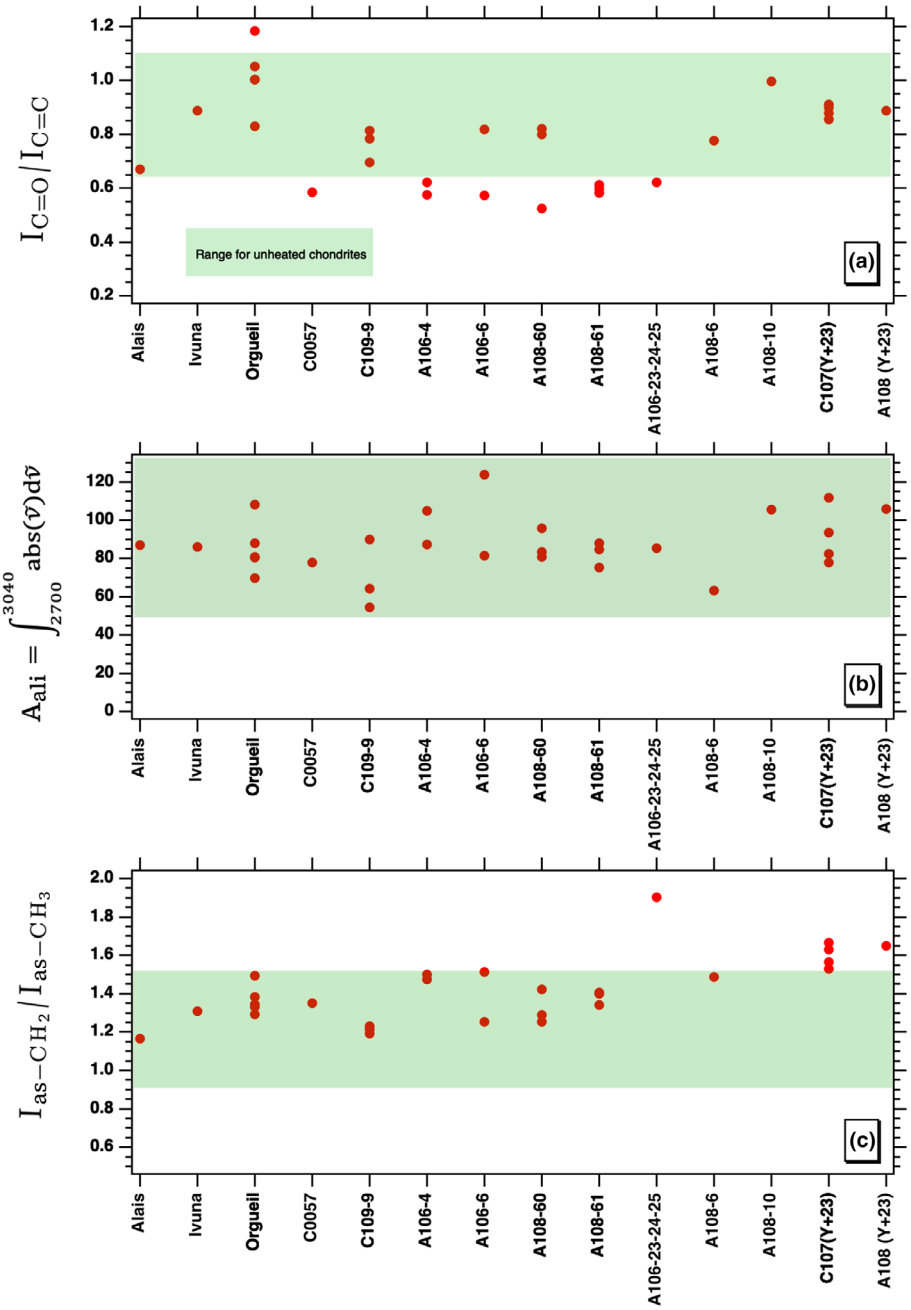

FIGURE 6. Three spectral parameters displayed for various IOM samples. (a) C=O band intensity is the ratio of the peak intensities of the C = O and C = C bands, at ~1700 and 1600 cm^{-1}, respectively; (b) $CH_2 + CH_3 + CH$ represents the integrated absorbance of the aliphatic band in the range 2800–3000 cm^{-1}, calculated in spectra with the C = C band peak set to 1; (c) I_{CH_2}/I_{CH_3} is the ratio of the peak intensities of the antisymmetric stretching modes of the CH_3 and CH_2 functional groups. The green rectangle depicts the range of variations of these parameters in the case of type 1 and 2 carbonaceous chondrites (Quirico et al., 2018). (Color figure can be viewed at wileyonlinelibrary.com)

and C0109-9 show integrated absorbances of the aliphatic band and I_{CH_2}/I_{CH_3} ratios comparable with values measured for IOM extracted from unheated CI, CM, and CR chondrites (Figure 6b,c). Within each sample, the parameters display significant variations, which are not correlated one with each other. The C = O abundance (Figure 6a) displays significant variations within each sample, and, interestingly, part of the values is below the lower limit of unheated chondrites, including CIs. A0106-23,24,25 departs from other sample because its I_{CH_2}/I_{CH_3}

lies in the range of heated chondrites. The integrated absorbance of the aliphatic band fits that of unheated chondrite.

Non-IOM Residues

The residues of A0108-6,10 consisted of dark opaque grains (no infrared spectra could be collected) and translucent orange-brownish grains aside (Z_2 and Z_1 zone, respectively, in Figure 8a). The spectra of these outlier carbonaceous phase residues look quite different from chondritic IOM: We interpret them as not being composed of typical chondritic IOM (Figure 7). For the first spectrum collected (top spectrum in Figure 7), the aliphatic band points to a high CH_2 abundance versus CH_3. We also observe a broad and intense asymmetric band peaking at 3244 cm^{-1}, which does not fit with adsorbed water. This band may be due to molecular water or hydroxyl trapped in some insoluble minerals. The C = C band also seems broader, but we cannot exclude a contribution of the bending mode of molecular water, if present. The second spectrum (just below the previous one in Figure 7) shows a faint aliphatic band with a high CH_2 asymmetric stretch and a shift of C=C bands from 1590 to 1614 cm^{-1}.

AFM-IR Measurements on A0108-6,10

As pointed in Non-IOM Residues Section, micro-FT-IR spectra were collected on translucent regions of A0108-6,10 (non-IOM residue), but no spectra could be obtained for the dark regions, probably because of the presence of abundant opaque insoluble sulfides. Consequently, AFM-IR measurements were performed on two regions of A0108-6,10: (1) Z_1, a thin (700–800 nm) yellowish translucent area; (2) Z_2, a thicker dark area (1000–1400 nm; Figure 8a).

Spectra of Z_1 collected in contact mode show a C=O band at 1712 cm^{-1} and a C=C band centered at ~1610 cm^{-1} (Figure 8b,c). The C=C band does not display a well-defined peak, rather a plateau, and its intensity is lower than that of the C=O band. We also observe the CH_2 and CH_3 bands at 1455 and 1379 cm^{-1}, respectively, and a broad congested feature with a maximum at ~1200 cm^{-1}, which is observed in spectra of IOM extracted from Ryugu grains and primitive chondrites (Figure 8c). The intensity of this broad feature, however, varies from sample to sample, and overall, AFM-IR spectra are not strictly similar to spectra collected with conventional micro-FT-IR, that show a lower intensity carbonyl C=O band, a C=C band with a well-defined peak, and a weaker, narrower broad congested band, centered around 1300 cm^{-1} (Figure 7).

The IR images at 1720, 1600, and 1450 cm^{-1}, corresponding to the C=O, C=C, and CH_2 bending mode and/or carbonate, were collected in the Z_1 area of 10×10 μm^2 (Figure 9b–d). The RGB composite map (Figure 9e) was obtained from these three images. Some particles display a strong absorption at 1450 cm^{-1} (Figure 9d,e), which is attributed to carbonate residues. The presence of carbonates is confirmed in spectra collected in contact mode (Figure 8c). We calculated the C=O/C=C ratio map from the two images collected at 1720 and 1600 cm^{-1} (Figure 9f) and obtained a histogram of the distribution of the $I_{C=O}/I_{C=C}$ parameter (Figure 9g). The $I_{C=O}/I_{C=C}$ ratio shows an asymmetric distribution with average and median values of 1.68 and 1.56, respectively. Spatial heterogeneity does not account for those differences between macro-FT-IR and AFM-IR spectra. Measurements on IOM extracted from the CR2 (EET 92042) and Orgueil chondrites, under similar instrumental conditions, also show a higher carbonyl band (Phan et al., 2022). Therefore, an instrumental effect is suspected here. Besides these organic features, carbonates and sulfates have also been identified. While sulfates could be due to oxidized insoluble sulfides, the presence of carbonates is intriguing as this species is not expected to survive the harsh acid treatment. A possible explanation is that it was encapsulated in organic matter, and then protected against hydrochloric acid. Entanglement at the nanometer scale of diffuse organic matter with calcite is reported in Ryugu particles, and it may account for subsequent encapsulation of carbonate grains during the HF/HCl protocol (Yabuta et al., 2023).

AFM-IR measurements on the Z_2 zone show the localized presence of sulfates (Z_2-I) (Figure 10). This opaque zone (Z_2-I) (to visible and infrared radiations) is rich in insoluble sulfides, which presumably got partially oxidized by terrestrial atmosphere. We observed that the ratio of C=O/C=C in Z_2-II is significantly higher than in Z_2-III. A broad feature between 1400 and 1800 cm^{-1} confirms the presence of C=C and C=O bonds in Z_2-III but the spectral congestion is here higher than in spectra of zone Z_1 (non-IOM residue), and higher than in micro-FT-IR spectra of Ryugu IOM, which are fairly similar to those of chondritic IOM. In addition, the congested spectral range between 1400 and 1000 cm^{-1} is also significantly different from the micro-FT-IR spectra of Ryugu IOM. It is then difficult to draw a firm conclusion about the nature of IOM in this sample. The spectral differences can be due to (1) actual spatial variation in IOM composition at the nanometer scale, or (2) instrumental effects, resulting in perturbations in the baseline. Even in samples containing few minerals like immature coals, strong variabilities in the baseline are observed and their source has not been yet identified (Phan et al., 2023).

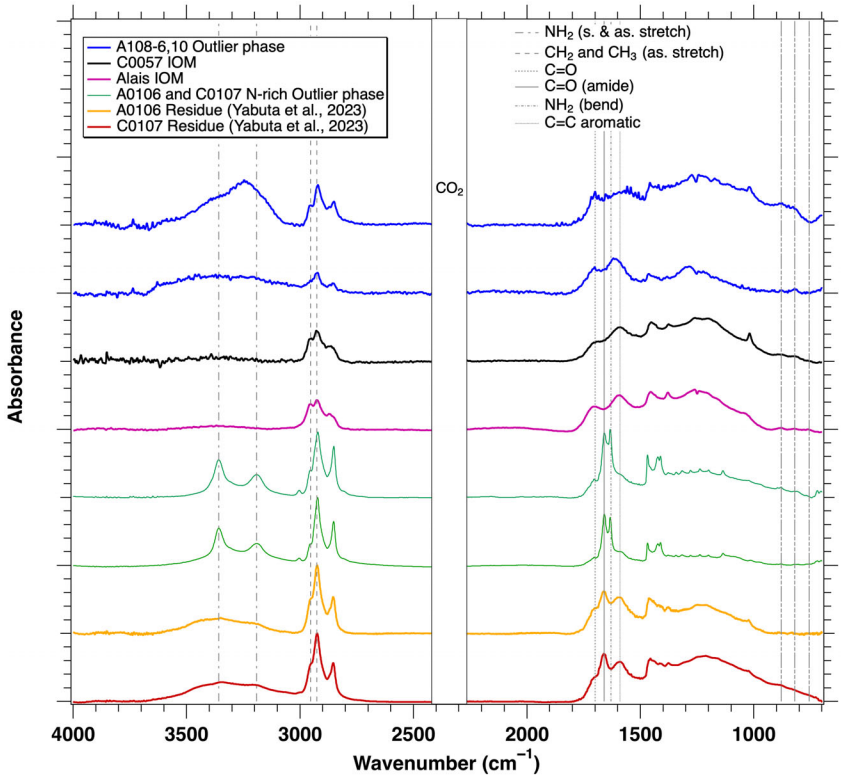

FIGURE 7. IOM baseline-corrected spectra of outlier phases recovered from A0108-6 and A0108-10 aggregates, displayed with the spectra of IOM samples extracted from C0057 and Alais. The figure also displays the spectra of the A0106 and C0107 residues from Yabuta et al. (2023), and N-rich outlier phases recovered from these residues, reported in Kebukawa et al. (2023). (Color figure can be viewed at wileyonlinelibrary.com)

Overall, AFM-IR measurements confirm the differences between the non-IOM residue in zone Z_1 and Ryugu IOM. In zone Z_2, the spectra of the darker and thicker residue show the C=O and C=C band, but the spectra do not match those of Ryugu IOM. It is difficult to get firm conclusions, regarding possible artifacts due to sample topography, porosity, and heterogeneity.

Bulk Grains from A0108 and C0109 Aggregates

IR spectra were measured on intact bulk particles from A0108-6, A0108-10, A0108-18, and C0109-12 aggregates (Figure 11). They are systematically dominated by the Si-O and OH stretching modes of Mg-rich phyllosilicates at 1010 and 3687 cm^{-1}. These features are remarkably consistent with those of Orgueil, and the SiO band is substantially different from that in CM chondrites, whose matrix is dominated by serpentines and proto-serpentines. This is consistent with the fact that Orgueil and Ryugu grains are dominated by Mg-rich serpentine and saponite (Nakamura et al., 2022; Tomeoka & Buseck, 1988). The narrow peak at 3687 cm^{-1} is accompanied by a shoulder due to, possibly, reminiscent molecular water in the interfoliar space of the saponite or closed porosity, or oxyhydroxide minerals. Note that Ryugu samples' dehydration in the environmental cell was very rapid (5–10 min), and that most of water was released at room temperature. This supports a high level of open porosity. A grouplet of three weak features at 1260, 1290, and 1306 cm^{-1} is also present, which is also observed in CI chondrites—but not in CM and CR chondrites. The nature of these bands is not elucidated.

Several bands due to organic species are clearly observed on the spectra acquired on bulk Ryugu samples: (1) the aliphatic band with peaks at 2956, 2925, 2869, and 2854 cm^{-1}, along with the CH_2 and CH_3 deformation modes at 1455 and 1380 cm^{-1} (in some spectra, the ν_3 vibration mode of carbonates contributes to the 1455 cm^{-1} band); (2) a signature at ~1620 cm^{-1}, assigned to the C=C stretching mode, with a possible contribution of the bending mode of molecular water; (3) a band in the range 1697–1689 cm^{-1}, assigned to the C=O group. The peak intensities of these features are variable. In particular, the intensity of the C=O band is much higher than the C=C band in several spectra, which does not match infrared spectra of IOM (Figures 4 and 5), thereby showing the contribution of soluble organic molecules.

The integrated absorbance of the aliphatic band and the ratio of the peak intensities of the asymmetric stretching modes of the CH_2 and CH_3 groups were computed (Figure 12). The aliphatic abundance displays

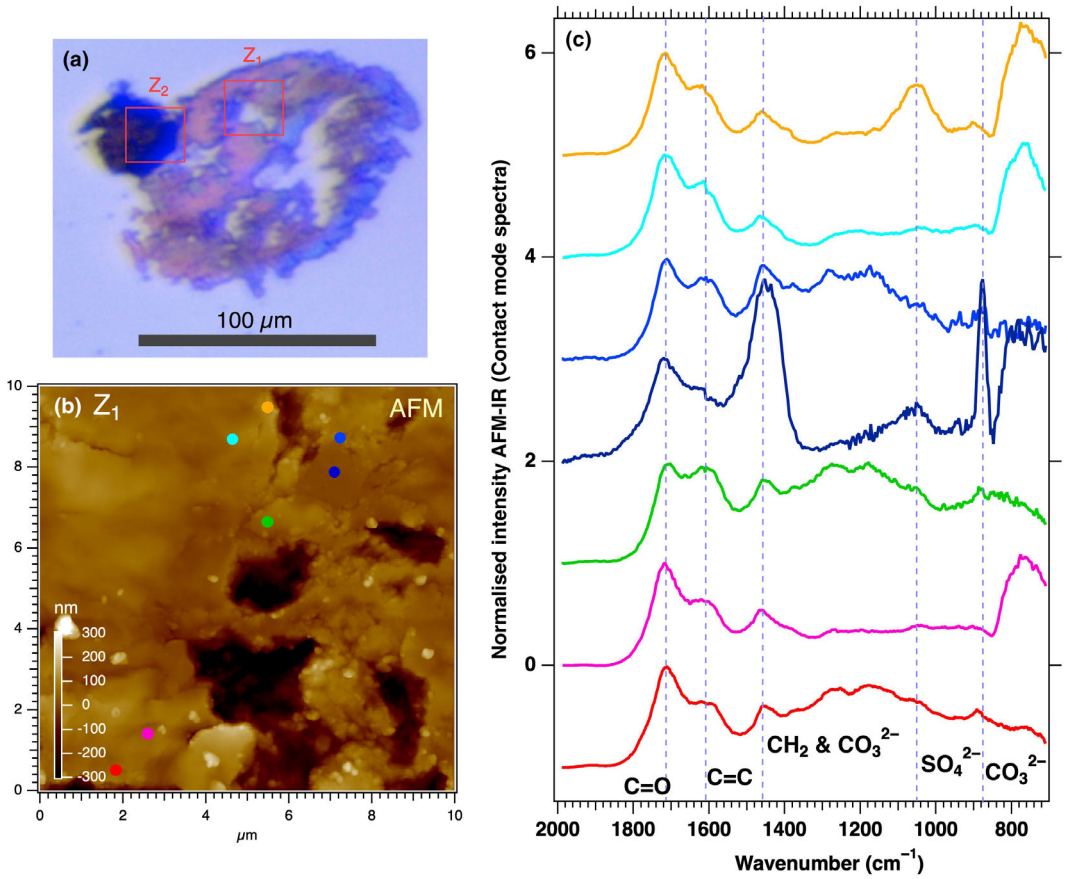

FIGURE 8. (a) Optical image showing the zones Z1 (translucent) and Z2 (dark/opaque). (b) AFM topographic image of zone Z1 and contact mode AFM-IR spectra (c) collected at locations pointed out by colored circles. Carbonates and sulfates are identified. Spectral variations are observed in the spectra of organic material, as the relative intensity of the C=O and C=C bands, and intensity of the broad feature centered around 1200 cm^{-1}. (Color figure can be viewed at wileyonlinelibrary.com)

a range of values that encompasses Orgueil and the MET01070, DOM 8003, and Tarda CM chondrites, and reach to higher values in the case of A0108-6 and A0108-10. In contrast, the CH_2/CH_3 ratio determined in raw matrix grains is higher than in IOM extracted from unheated CI, CM, and CR chondrites which is consistent with the calculation from Dartois et al. (2023). Altogether, this supports the view that the spectra of Ryugu bulk grains reflect both the insoluble and soluble organic components.

DISCUSSION

IOM Samples and Post-Accretional Processes

We first remind the main conclusions from the Results section:

- Infrared spectra of IOM samples extracted from Ryugu grains match those of IOM extracted from unheated type 1 and 2 chondrites, except the spectrum of the IOM of A0108-23,24,25. Their aliphatic abundance and CH_2/CH_3 ratio display variations within the range of variations of unheated CI/CM/CR chondrites (Quirico et al., 2018). We note, however, significant variations of these parameters within and across samples.
- The C=O/C=C ratio (carbonyl abundance) in IOM of C0057-9, A0106-4, A0106-6, A0108-60, A0108-61, and A0106-23-24-25 displays lower values than those in unheated chondrites (Figure 6a). Not all oxygen is present in carbonyl groups in chondritic IOM, and ether and alcohol groups are major functional groups (Cody & Alexander, 2005). Nevertheless, this low C=O abundance in some particles of Ryugu IOM is consistent with the O/C ratio estimated by NanoSIMS (0.12 and 0.04 for chambers A and C, respectively), and by STEM-EDS analyses (0.1 for both chambers A and C; Yabuta et al., 2023), which are both lower than O/C in Orgueil and Ivuna IOM samples, as 0.18 ± 0.02 and 0.158, respectively (Alexander et al., 2007).

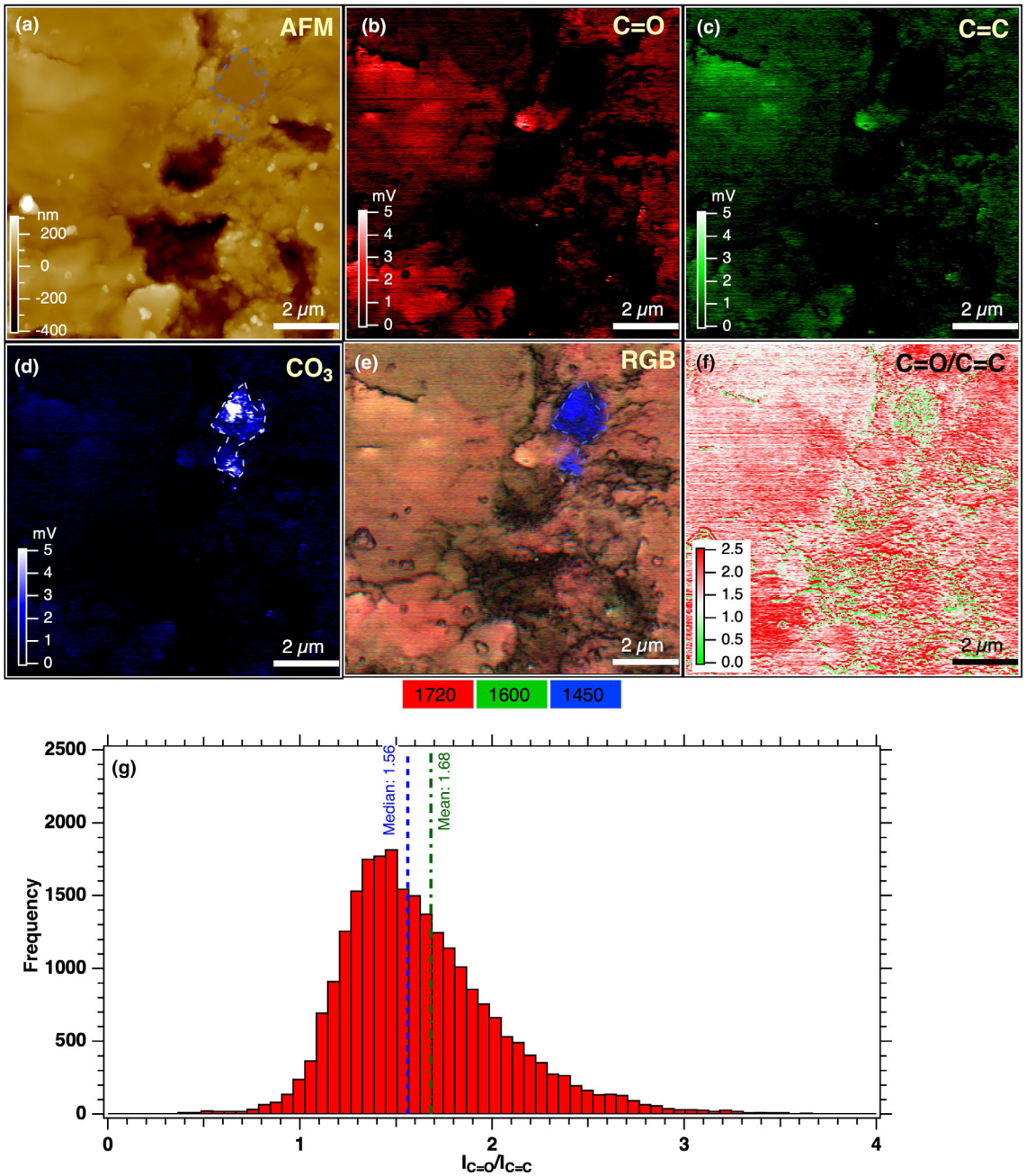

FIGURE 9. AFM-IR measurements in zone Z_1. (a) AFM topographic image. Absorption image at (b) 1720 cm^{-1}, (c) 1600 cm^{-1}, (d) 1450 cm^{-1}, (e) composite RGB image built from tapping mode images collected at 1720, 1600, and 1450 cm^{-1}, (f) intensity ratio map between 1720 and 1600 cm^{-1}. Carbonates are present after the acid extraction indicated by the dashed line area, (g) histogram of $I_{C=O}/I_{C=C}$ measured from images collected at 1720 and 1600 cm^{-1} in tapping mode in (f). (Color figure can be viewed at wileyonlinelibrary.com)

- A0106-23,24,25 is in contrast different than other samples as it displays a CH_2/CH_3 ratio consistent with a mild heating stage, but the C=O band has a similar intensity than that in other samples.
- No systematic difference is observed between chambers A and C.

It is well established that thermal metamorphism (whatever of short or long duration) leads to decarbonylation of terrestrial and extraterrestrial IOM (Kebukawa et al., 2011; Orthous-Daunay et al., 2013; Vanderbroucke & Largeau, 2007). Even some type 1 and 2 chondrites have experienced heating on their parent

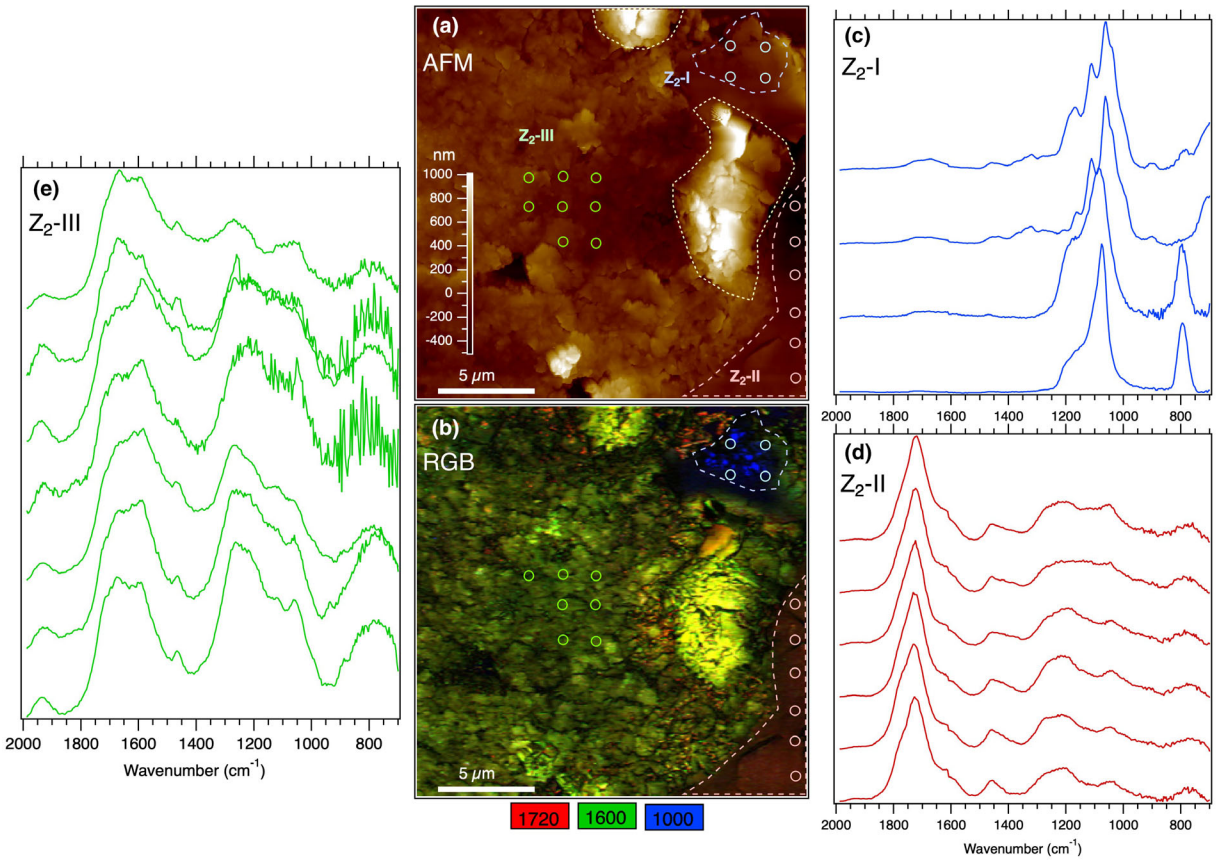

FIGURE 10. AFM-IR measurements in zone Z2. (a) AFM topographic image. (b) Composite RGB image built from tapping mode images collected at 1000, 1600, and 1720 cm^{-1}. The colored circles point to contact mode spectra presented in (c–e). Sulfates are present as presumably oxidation byproducts of native sulfides in atmosphere. AFM-IR spectra of organic material display the C=O and C=C bands, but show significant differences with Ryugu IOM spectra collected by micro-FT-IR. Artifacts due to sample preparation may account for these differences. (Color figure can be viewed at wileyonlinelibrary.com)

body, making the old classification of Van Schmus and Wood (1967) obsolete because thermal metamorphism and hydrothermal alteration are independent processes (Nakamura, 2005; Quirico et al., 2018; Tonui et al., 2014). Bonal et al. (2024) searched for evidence of parent body heating through the characterization of the sp^2 structure of IOM by Raman spectroscopy (aggregates A0106-4; A0106-6; A0106-23,24,25; A0108-6; A0108-10; A0108-61; C0109-5; C0109-9; C0109-12; and individual particle C0057-6). Measurements were collected on each intact particle and on a few extracted IOM from A0106-23,24,25; A0108-10; C0109-12; and C0057-6. The results show that most samples correspond to unheated material, that is, which was not thermally processed on the parent body, in agreement with the temperature estimate of 37 ± 10°C derived from oxygen isotopes (Yokoyama et al., 2023). C0109-9 and A0108-10 display Raman parameters out of the trend of unheated chondrites, but infrared spectra do not point to thermal stress in the case of C0109-9 (no infrared data are available for A0108-10). This discrepancy could be due to the fact that Raman and infrared analysis are not co-located, and that this grain may have some structural heterogeneity. This explanation could also hold for the sample A0106-23,24,25, rated as unheated by the Raman analysis and slightly heated by infrared data. An alternate explanation is that IOM could have been compositionally modified by short duration heating without detectable structural evolution. This case was observed once by Quirico et al. (2018) in the case of the CM2 MIL 07700 (one occurrence out of 40 samples). The IOM of this chondrite is structurally similar to an unheated chondrite, but has been thermally processed according to its chemical composition.

Cratering and heating due to micrometeorite impacts could account for some heterogeneous heating at the micrometric scale (Noguchi et al., 2023). Impact features, as layers and melt splashes, are observed for ~6% of analyzed Ryugu particles. Smooth layers, the most abundance impact feature, are very thin (<100 nm) and cannot account for a significant chemical change in a 500 μm particle. Evidence of melting is vesicles and immiscible separation of rounded (once molten) sulfides

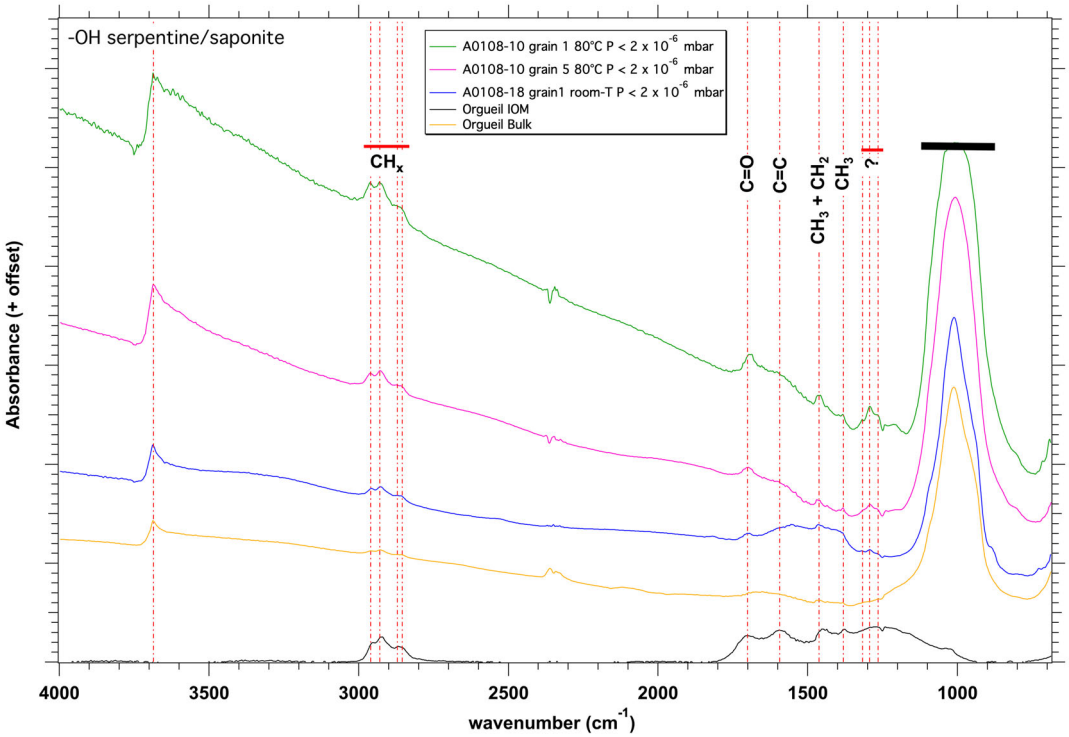

FIGURE 11. Infrared spectra of grains picked up from A0108-10 and A0108-18 aggregates, compared to Orgueil grains and an IOM sample. Spectra were not baseline-corrected. Note that the SiO band is saturated for the sample A0108-10 grain 1. We observe a very good match between Ryugu and Orgueil bulk grains. The organic features in the spectra of raw grains point to the presence of a significant soluble organic matter phase, which is more abundance in Ryugu grains compared to Orgueil. (Color figure can be viewed at wileyonlinelibrary.com)

(Noguchi et al., 2023). This shows that hypervelocity impacts trigger a significant heating in exposed particles. Still, these features are localized at the surface of the particles and do not reach the interior of large 500 μm grains, and micrometeorite impacts appear as a limited source of heating. In conclusion, A0106-23-24-25 has possibly experienced a very moderate short-duration heating, but other samples have not. Therefore, the lower carbonyl abundance in Ryugu IOM cannot be explained by short duration heating on the parent body.

Hydrothermal alteration on the parent body is an oxidative process, and it possibly results in the formation of carbonyl groups. Our data point to the following trend in carbonyl abundance: Ryugu < Alais < Ivuna ~ Orgueil. Interestingly, Endreß and Bischoff (1996) propose an increasing degree of aqueous alteration as Alais < Ivuna < Orgueil, based on the composition of carbonates. Suga et al. (2022) report a heterocyclic sulfur abundance in Ryugu IOM closer to that in CMs than in CI falls. This form of organic sulfur is found to increase with the extent of aqueous alteration (Orthous-Daunay et al., 2010), which supports a lower degree of aqueous alteration for Ryugu samples. However, the carbonyl abundance in primitive CMs and CRs is higher than in Ryugu samples and lies within the range of CIs, though they have experienced a lower degree of hydrothermal alteration (in particular the primitive CR2 chondrites). In addition, most of IOM extracted from CM and CR primitive chondrites show an O/C elemental ratio of their IOM consistent with those of CI chondrites (Alexander et al., 2007). Therefore, there is no clear relation between carbonyl abundance and degree of aqueous alteration.

Oxidation through terrestrial weathering has been reported as a source of alteration of IOM in primitive chondrites, in particular for desert finds (Alexander et al., 2007). The formation of carbonyl groups in IOM from exposition of moisture and atmospheric oxygen is in fact not consistent with the presence of a low carbonyl abundance in type 2 chondrites that have experienced a very mild degree of heating. In that case, the polyaromatic structure and composition of IOM experienced very limited chemical modifications and we expect a similar sensitivity to oxidation than an immature IOM extracted from an unheated chondrite. In addition, it is well known in organic geochemistry that kerogens are stabilized when trapped in their host rock, while they are very reactive once extracted and require stringent storage conditions (Vandenbroucke & Largeau, 2007). We also argue that CI falls Alais, Orgueil, and Ivuna fell, respectively, on 1806, 1864, and 1938, and no link is

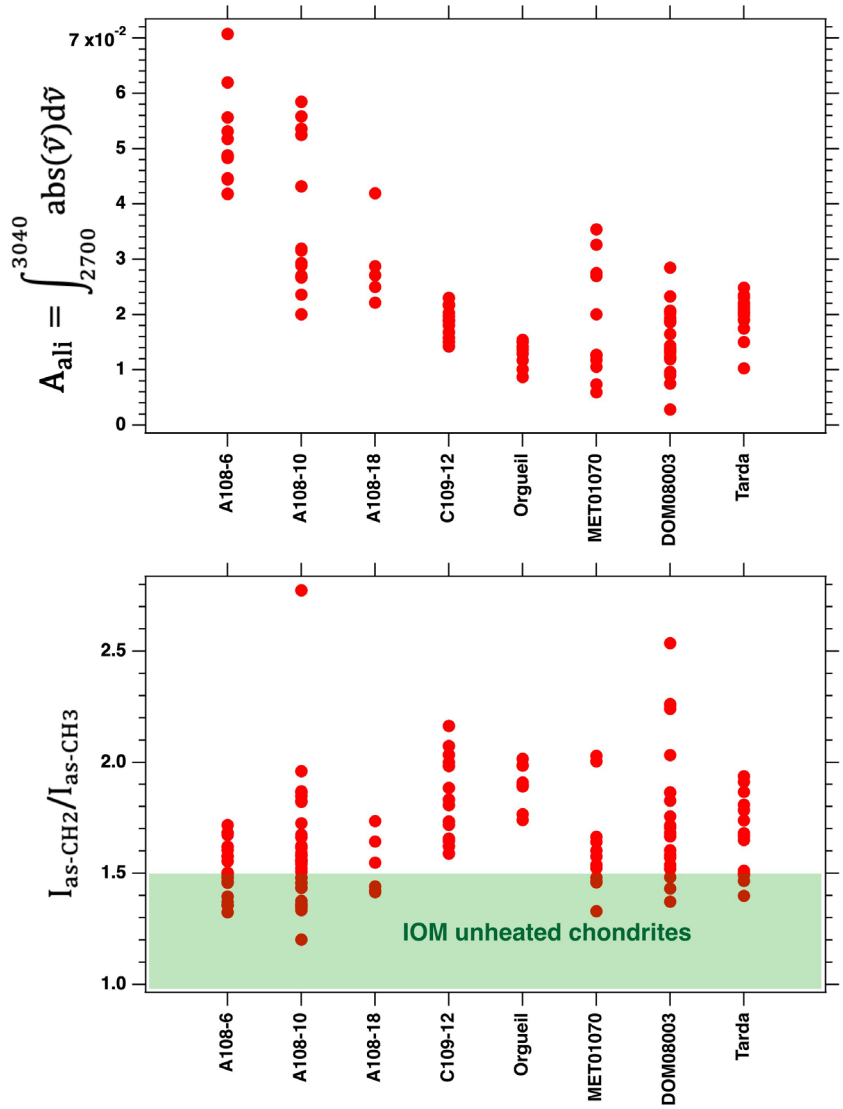

FIGURE 12. Top: The integrated absorbance of the 2800–300 cm^{-1} aliphatic band, calculated from IOM baseline-corrected spectra of various aggregates and individual grains (the peak intensity of the SiO band was set to 1). Bottom: The ratio of the peak intensities of the antisymmetric stretching modes of the CH_3 and CH_2 functional groups. Ryugu grains tend to show a higher aliphatic abundance compared to carbonaceous chondrites Orgueil, MET 01070, DOM 08003, and Tarda. The higher values of I_{CH_2}/I_{CH_3} compared to IOM show the significant contribution of SOM. (Color figure can be viewed at wileyonlinelibrary.com)

observed between IOM composition and residence time on Earth (Orthous-Daunay et al., 2010, 2013).

Finally, the most plausible explanation is that Ryugu accreted less oxygenated organic precursors than primitive chondrites, including CI falls.

Comparison with Other IOM, Outlier Carbonaceous Phases

IOM extracted from micrometer-sized Ryugu particles in this study displays significant differences compared to IOM samples Y23-A0106-IOM and Y23-C0107-IOM of Yabuta et al. (2023), but look similar to the IOM extracted from the large particle C0002 presented in Kebukawa et al. (2023) (Figure 8). 13.08, 10.73, and 3 mg of Ryugu samples were used for producing Y23-A0106-IOM, Y23-C0107-IOM, and C0002 IOM samples, respectively. In contrast, each grain in our study corresponds to around 100 μg (assuming a spherical particle with a 500 μm diameter and 2 g cm^{-3} density). In this respect, Y23-C0107-IOM and Y23-A0106-IOM would appear more representative of the whole Ryugu material. However, the similarity of C0002 IOM with IOM samples extracted in this study supports that Ryugu IOM is similar to that of primitive unheated chondrites.

Kebukawa et al. (2023) report the spectra of an N-rich outlier carbonaceous phase, which fairly matches with some simple aliphatic amides (e.g., hexanamide). Several of the features of this phase are present in the spectra of Y23-A0106-IOM and Y23-C0107-IOM, that is, the amine stretching modes at 3188 and 3355 cm^{-1}, and the 1665 cm^{-1} mode (Figure 7). In addition, their higher CH_2/CH_3 can be accounted for by a contribution of the aliphatic bands of the outlier carbonaceous phase. Finally, Y23-A0106-IOM and Y23-C0107-IOM appear to be a mixture of IOM and this outlier nitrogen-rich soluble phase.

A main question that arises is the origin of the N-rich outlier phase. SOM in Ryugu samples is very similar to that in Murchison, and consists of a very complex mixtures of CHONS molecules, with ~20,000 chemical formulae identified (Naraoka et al., 2023). The abundant small molecules detected so far are formic and acetic acids, amino acids, nitrogenated bases, amines, and aromatic hydrocarbons (Naraoka et al., 2023; Oba et al., 2023; Parker et al., 2023).

In the extractions achieved in this study, outlier phases have been observed for two grains only, and their spectra are consistent with a low nitrogen abundance (no amine, cyanide, or amide bands) and a mixture of several molecules (Figure 7). Two explanations can be then proposed. The first would argue that the N-rich outlier phase has a special affinity to minerals, for instance saponite (Viennet et al., 2023), and could have been preferentially preserved during SOM extraction by hot water. It would have been released during the HF/HCl sequence due to silicates hydrolysis, and finally mixed up with IOM. The second explanation would argue that this phase is a contamination during the hot water extraction. However, the SOM analyses conducted in the PET SOM did not report a high abundance of this compound (Naraoka et al., 2023).

IOM Features in the Spectra of Intact Grains?

Regarding the spectra collected on intact grains (Figure 11), the infrared spectra of grains A0108-6, A0108-10, A0108-18, and C0109-12 display organic features as: CH_2 and CH_3 stretching (2956, 2925, 2869, 2854 cm^{-1}), bending and deformation modes (1455 and 1380 cm^{-1}), carbonyl (~1700 cm^{-1}), and C=C stretching modes (~1600 cm^{-1}). These features cannot be assigned to the sole IOM. The peak ratio of the antisymmetric stretching modes of CH_2 and CH_3 is higher than that of IOM (Figures 11 and 12), consistently with the results of Dartois et al. (2023). The aromatic C=C band is also weaker, and the broad congested band in the range 800–1500 cm^{-1} does not appear. Most likely, SOM significantly contributes to the spectra of raw grains, and extracting the actual signatures of IOM is not straightforward.

CONCLUSION

In this study, we chemically extracted IOM from a series of submillimeter Ryugu samples by means of acid leaching in a dedicated experimental device. The residues were analyzed by infrared microscopy. The main conclusions are the following:

1. IOM extracted from most of the samples look very similar to IOM extracted from unheated CI, CM, and CR chondrites.
2. The extent of heating in Ryugu regolith appears very limited: Only one sample displays chemical signatures consistent with a very mild heating.
3. Infrared measurements show overall a lower carbonyl abundance in Ryugu IOM samples, which appears consistent with the lower O/C elemental ratio determined by NanoSIMS and STEM-EDS analyses reported in Yabuta et al. (2023).
4. This lower carbonyl abundance is not easily explained by a lower extent of hydrothermal alteration on the parent body, nor by carbonyl formation in primitive chondrites by oxidation due to terrestrial weathering. The accretion of carbonyl-poor precursors by Ryugu is a plausible explanation.
5. The spectra of raw grains display signatures of organic materials due to both the IOM and SOM components, whose respective contributions are very hard to disentangle. Their very strong similarities with the spectra of the CI chondrites Alais, Ivuna, and Orgueil reinforce the view that Ryugu samples are genetically related to this class of chondrites.
6. Some of our IOM extractions led to outlier carbonaceous phases, but with different (N-poor) compositions to that reported in Kebukawa et al. (2023).
7. The residues presented in Yabuta et al. (2023) are in fact not pure IOM, but include a contribution from the nitrogen-rich outlier carbonaceous phase.

Acknowledgments—This study was funded by the French space agency CNES (Centre National d'Etudes Spatiales). This research was also supported by the H2020 European Research Council (ERC) (SOLARYS ERC-CoG2017_771691). We are very grateful to Mike Zolensky and an anonymous reviewer for constructive and helpful comments that have greatly improved the manuscript.

Data Availability Statement—Our data will be made accessible to anyone through the SSHADE database:

https://www.sshade.eu/A doi link has been indicated in the manuscript, and will get activated after acceptation of the article by Wiley.

Editorial Handling—Dr. Edward Anthony Cloutis

REFERENCES

Alexander, C. M. O'D., Fogel, M., Yabuta, H., and Cody, G. D. 2007. The Origin and Evolution of Chondrites Recorded in the Elemental and Isotopic Compositions of their Macromolecular Organic Matter. *Geochimica et Cosmochimica Acta* 71: 4380–4403.

Battandier, M., Bonal, L., Quirico, E., Beck, P., Engrand, C., Duprat, J., and Dartois, E. 2018. Characterization of the Organic Matter and Hydration State of Antarctic Micrometeorites: A Reservoir Distinct from Carbonaceous Chondrites. *Icarus* 306: 74–93.

Bonal, L., Quirico, E., Montagnac, G., Komatsu, M., Kebukawa, Y., Yabuta, H., Amano, K., et al. 2024. The Thermal History of Ryugu Based on Raman Characterization of Hayabusa2 Samples. *Icarus* 408: 115826.

Chen, Y., Mastalerz, M., and Schimmelmann, A. 2012. Characterization of Chemical Functional Groups in Macerals across Different Coal Ranks Via Micro-FTIR Spectroscopy. *International Journal of Coal Geology* 104: 22–33. https://doi.org/10.1016/j.coal.2012.09.001.

Cody, G. D., and Alexander, C. M. O'D. 2005. NMR Studies of Chemical Structural Variation of Insoluble Organic Matter from Different Carbonaceous Chondrite Groups. *Geochimica et Cosmochimica Acta* 69: 1085–97. https://doi.org/10.1016/j.gca.2004.08.031.

Dartois, E., Caro, G. M. M., Deboffle, D., Montagnac, G., and d'Hendecourt, L. 2005. Ultraviolet Photoproduction of ISM Dust. *Astronomy and Astrophysics* 432: 895–908.

Dartois, E., Engrand, C., Brunetto, R., Duprat, J., Pino, T., Quirico, E., Remusat, L., et al. 2013. UltraCarbonaceous Antarctic Micrometeorites, Probing the Solar System beyond the Nitrogen Snow-Line. *Icarus* 224: 243–252.

Dartois, E., Kebukawa, Y., Yabuta, H., Mathurin, J., Engrand, C., Duprat, J., Be-Jach, L., et al. 2023. Chemical Composition of Carbonaceous Asteroid Ryugu from Synchrotron Spectroscopy in the Mid- to Far-Infrared of Hayabusa2-Returned Samples. *Astronomy and Astrophysics* 671: A2.

Dartois, E., Munoz Caro, G. M., Deboffle, D., and D'Hendecourt, L. 2004. Diffuse Interstellar Medium Organic Polymers Photoproduction of the 3.4, 6.85 and 7.25 mm Features. *Astronomy and Astrophysics* 423: 33–36.

Durand, B., and Nicaise, G. 1980. Procedures of Kerogen Isolation. In *Kerogen: Insoluble Organic Matter from Sedimentary Rocks*, edited by B. Durand, 35–53. Paris: Editions Technip.

Endreß, M., and Bischoff, A. 1996. Carbonates in CI Chondrites: Clues to Parent Body Evolution. *Geochimica et Cosmochimica Acta* 60: 489–507.

Ito, M., Tomioka, N., Uesugi, M., Yamaguchi, A., Shirai, N., Ohigashi, T., Liu, M. C., et al. 2022. A Pristine Record of Outer Solar System Materials from Asteroid Ryugu's Returned Sample. *Nature Astronomy* 6: 1163–71.

Kebukawa, Y., Alexander, C. M. O'D., and Cody, G. D. 2011. Compositional Diversity in Insoluble Organic Matter in Type 1, 2 and 3 Chondrites as Detected by Infrared Spectroscopy. *Geochimica et Cosmochimica Acta* 75: 3530–41.

Kebukawa, Y., Quirico, E., Dartois, E., Yabuta, H., Bejach, L., Bonal, L., Dazzi, A., et al. 2023. Infrared Absorption Spectra from Organic Matter in the Asteroid Ryugu Samples: Some Unique Natures Compared to Unheated Carbonaceous Chondrites. *Meteoritics & Planetary Science* 1–14. https://doi.org/10.1111/maps.14064.

Kitazato, K. R. E., Milliken, T., Iwata, M., Abe, M., Ohtake, S., Matsuura, T., Arai, Y., et al. 2019. The Surface Composition of Asteroid 162173 Ryugu from Hayabusa2 Near-Infrared Spectroscopy. *Science* 364: 272–75.

Lin-Vien, D., Norman, B. C., William, G. F., and Grasselli, J. G. 1991. *The Handbook of Infrared and Raman Characteristic Frequencies of Organic Molecules*. New York: Academic Press.

MacPhail, R. A., Strauss, H. L., Snyder, R. G., and Eiliger, C. A. 1984. C-H Stretching Modes and the Structure of n-Alkyl Chains. 2. Long, all-Trans Chains. *The Journal of Physical Chemistry* 88: 334–341. https://doi.org/10.1021/j150647a002.

Nakamura, T. 2005. Post-Hydration Thermal Metamorphism of Carbonaceous Chondrites. *Journal of Mineralogical and Petrological Sciences* 100: 260–272.

Nakamura, T., Matsumoto, M., Amano, K., Enokido, Y., Zolensky, M. E., Mikouchi, T., Genda, H., et al. 2022. Formation and Evolution of Carbonaceous Asteroid Ryugu: Direct Evidence from Returned Samples. *Science* 379: eabn8671. https://doi.org/10.1126/science.abn8671.

Naraoka, H., Takano, Y., Dworkin, J. P., Oba, Y., Hamase, K., Furusho, A., Ogawa, N. O., et al. 2023. Soluble Organic Molecules in Samples of the Carbonaceous Asteroid (162173) Ryugu. *Science* 379: 789.

Noguchi, T., Matsumoto, T., Miyake, A., Igami, Y., Haruta, M., Saito, H., Hata, S., et al. 2023. A Dehydrated Space-Weathered Skin Cloaking the Hydrated Interior of Ryugu. *Nature Astronomy* 7: 170–181. https://doi.org/10.1038/s41550-022-01841-6.

Oba, Y., takano, Y., Dworkin, J. P., and Naraoka, H. 2023. Ryugu Asteroid Sample Return Provides a Natural Laboratory for Primordial Chemical Evolution. *Nature Communications* 14: 3107.

Okazaki, R., Miura, Y. N., Takano, Y., Sawada, H., Sakamoto, K., Yada, T., Yamada, K., et al. 2022. First Asteroid Gas Sample Delivered by the Hayabusa2 Mission: A Treasure Box from Ryugu. *Science Advances* 8: eabo7239.

Orthous-Daunay, F. R., Quirico, E., Beck, P., Brissaud, O., Dartois, E., Pino, T., and Schmitt, B. 2013. Mid-Infrared Study of the Molecular Structure Variability of Insoluble Organic Matter from Primitive Chondrites. *Icarus* 223: 534–543.

Orthous-Daunay, F.-R., Quirico, E., Lemelle, L., Beck, P., de Andrade, V., Simionovici, A., and Derenne, S. 2010. Speciation of Sulfur in the Insoluble Organic Matter from Carbonaceous Chondrites by XANES Spectroscopy. *Earth and Planetary Science Letters* 300: 321–28. https://doi.org/10.1016/j.epsl.2010.10.012.

Painter, P. P., Snyder, R. W., Starsinic, M., Coleman, M. M., Kuehn, D. W., and Davis, A. 1981. Concerning the Application of FT-IR to the Study of Coal: A Critical Assessment of Band Assignments and the Application of

Spectral Analysis Programs. *Applied Spectroscopy* 35: 475–485. https://doi.org/10.1366/0003702814732256.

Parker, E. T., McLain, H. L., Glavin, D. P., Dworkin, J. P., Elisa, J. E., Aponte, J. C., Naraoka, H., et al. 2023. Extraterrestrial Amino Acids and Amines Identified in Asteroid Ryugu Samples Returned by the Hayabusa2 Mission. *Geochimica et Cosmochimica Acta* 347: 42–57.

Petersen, H. I., Rosenberg, P., and Nytoft, H. P. 2008. Oxygen Groups in Coals and Alginite-Rich Kerogen Revisited, Coal. *Geology* 74: 93–113. https://doi.org/10.1016/j.coal.2007.11.007.

Phan, V. T. H., Quirico, E., Beck, P., Le Brech, Y., Jovanovic, L., Le Guillou, C., Bernard, S., et al. 2021. Infrared Spectroscopy Quantification of Functional Carbon Groups in Kerogens and Coals: A Calibration Procedure. *Spectrochimica Acta Part A: Molecular and Biomolecular Spectroscopy* 259: 119853.

Phan, V. T. H., Rebois, R., Beck, P., Quirico, E., Bonal, L., and Noguchi, T. 2022. Na-Noscale Mineralogy and Organic Structure in Orgueil (CI) and EET 92042 (CR) Carbonaceous Chondrites Studied with AFM-IR Spectroscopy. *Meteoritics & Planetary Science* 57: 3–21.

Phan, V. T. H., Rebois, R., Beck, P., Quirico, E., Noguchi, T., and Takase, M. 2023. Chemical Functional Characterization of Immature and Mature Coals at the Nanoscale by Atomic Force Microscopy-Based Infrared Spectroscopy (AFM-IR). *International Journal of Coal Geology* 267: 104196.

Quirico, E., Bonal, L., Beck, P., Alexander, C. M. O. D., Yabuta, H., Nakamura, T., Nakato, A., et al. 2018. Prevalence and Nature of Heating Processes in CM and C2-Ungrouped Chondrites as Revealed by Insoluble Organic Matter. *Geochimica et Cosmochimica Acta* 241: 17–37.

Suga, H., Tamenori, Y., Yabuta, H., Yurimoto, H., Nakamura, T., Noguchi, T., Okazaki, R., et al. 2022. Sulfur-XANES of Intact Ryugu Grains and the Isolated IOM. Hayabusa 2 Symposium, JAXA, Sagamihara, November 14–16.

Sugita, S., Honda, R., Morota, T., Kameda, S., Sawada, H., Tatsumi, E., Yamada, M., et al. 2019. The Geomorphology, Color, and Thermal Properties of Ryugu: Implications for Parent-Body Processes. *Science* 364: 6437. https://doi.org/10.1126/science.aaw0422.

Tomeoka, K., and Buseck, P. R. 1988. Matrix Mineralogy of the Orgueil CI Carbonaceous Chondrite. *Geochimica et Cosmochimica Acta* 52: 1627–40. https://doi.org/10.1016/0016-7037(88)90231-1.

Tonui, E., Zolensky, M., Hiroi, T., Nakamura, T., Lipschutz, M. E., Wang, M.-S., and Okudaira, K. 2014. Petrographic, Chemical and Spectroscopic Evidence for Thermal Metamorphism in Carbonaceous Chondrites I: CI and CM Chondrites. *Geochimica et Cosmochimica Acta* 126: 284–306.

Vanderbroucke, M., and Largeau, C. 2007. Kerogen Origin, Evolution and Structure. *Organic Geochemistry* 38: 719–833.

Van Schmus, W. R., and Wood, J. A. 1967. A Chemical-Petrologic Classification for the Chondritic Meteorites. *Geochimica and Cosmochimica Acta* 31: 747–765.

Viennet, J.-C., Roskosz, M., Nakamura, T., Beck, P., Baptiste, B., Lavina, B., Alp, E. E., et al. 2023. Interaction between Clay Minerals and Organics in Asteroid Ryugu. *Geochemical Perspective Letters* 25: 8–12.

Watanabe, S., Hirabayashi, M., Hirata, N., Hirata, N., Noguchi, R., Shimaki, Y., Ikeda, H., et al. 2019. Hayabusa2 Arrives at the Carbonaceous Asteroid 162173 Ryugu: A Spinning Top Rubble Pile. *Science* 364: 268–272.

Yabuta, H., George, D., Cody, C. E., Kebukawa, Y., De Gregorio, B., Bonal, L., Remusat, L., et al. 2023. Macromolecular organic matter in samples of the asteroid (162173) Ryugu. *Science* 379: eabn9057.

Yada, T., Abe, M., Okada, T., Nakato, A., Yogata, K., Miyazaki, A., Hatakeda, K., et al. 2022. Preliminary Analysis of the Hayabusa2 Samples Returned from C-Type Asteroid Ryugu. *Nature Astronomy* 6: 214–220.

Yokoyama, T., Nagashima, K., Nakai, I., Young, E. D., Abe, Y., Aléon, J., Conel, M. O'D., et al. 2023. Samples Returned from the Asteroid Ryugu Are Similar to Ivuna-Type Carbonaceous Meteorites. *Science* 379: 786. https://doi.org/10.1126/science.abn7850.